Fire Behaviour of Polydimethylsiloxane Materials for Spacecraft Applications

69th International Astronautical Congress (IAC), Bremen, Germany, 1-5 October 2018.

IAC-18,A2,4,1,x46032

Fire Behaviour of Polydimethylsiloxane Materials for Spacecraft Applications

U. Rojas-Alva[a]*, C. Creamer[a], D. Hanna[a], G. Jomaas[a]

[a]*School of Engineering, Institute for Environment and Infrastructure, University of Edinburgh, Thomas Bayes Road, The King's Buildings, Edinburgh, United Kingdom*
u.rojas-alva@ed.ac.uk
* Corresponding Author

Abstract

Flame spread experiments under opposed and concurrent buoyant and forced flows were conducted in a flow tunnel rig. The aim of the study was to understand the flame spread behaviour of Polydimethylsiloxane (PDMS) membrane sheets. The sample dimensions were 30 cm x 5 cm, and various thicknesses were considered in the study (0.125, 0.25, 0.36 and 0.61 mm). The results showed that burnt length (used as a criterion for NASA-STD-Test 1) is dependent on the forced flow direction and the forced flow velocity. The flame spread rate under opposed forced flow was independent of the forced flow, and the theoretical model showed good accuracy. In the concurrent case, the flame spread rate showed linear or non-monotonically dependency on forced flow. Quantification of the silica-ash formation upstream from the point of extinguishment exhibited a dependency on the concurrent forced flow. Flame spread of the PDMS under concurrent flows needs to consider kinetics to fully understand the role of silica-ash during burning.

Keywords: Flame spread, Buoyancy, Opposed, Concurrent, Silica-ash

Nomenclature

c_g	Specific heat capacity of gas $[J/kg.K]$
c_s	Specific heat capacity of solid $[J/kg.K]$
Bi	Biot number [-]
h_c	Convective heat transfer coefficient $[W/m^2K]$
L_{burnt}	Burnt length [cm]
l_{gx}	Gas-phase diffusion length in x-axis $[cm]$
l_{gy}	Gas-phase diffusion length in y-axis $[cm]$
l_f	Flame length $[cm]$
l_p	Pyrolysis length $[cm]$
l_r	Characteristic thermal length $[cm]$
$\dot{q}''_{cf}$	Convective heat flux from the flame to solid $[W/m^2]$
$\dot{q}''_{fr}$	Radiant flux from the flame to the solid $[W/m^2]$
$\dot{q}''_{sr}$	Re-radiation from the solid surface $[W/m^2]$
T_f	Flame temperature $[K]$
T_v	Vaporisation temperature $[K]$
T_∞	Ambient temperature $[K]$
V_g	Forced flow rate $[cm/s]$
V_{nb}	Characteristic induced forced flow due to natural buoyancy $[cm/s]$
V_f	Flame spread rate $[cm/s]$
x_{ext}	Distance from point of extinguishment [cm]

Greek Symbols

α_g	Thermal diffusivity of gas at T_v $[m^2/s]$
δ_{SiO_2}	Silica-ash thickness $[\mu m]$
λ_g	Conductivity of gas-phase $[W/m \cdot K]$
λ_s	Conductivity of solid-phase $[W/m \cdot K]$
τ_{crit}	Half critical thickness for thermal behaviour [cm]
τ	Half solid thickness [cm]
ρ_g	Density of gas-phase at T_v $[kg/m^3]$
ρ_s	Density of solid-phase $[kg/m^3]$

Acronyms/Abbreviations

NASA	National Aeronautics and Space Administration
PDMS	Polydimethylsiloxane
Saffire	Spacecraft Fire Experiments
SEM	Scanning Electron Microscope

1. Introduction

Space exploration is no longer an activity reliant on the Government of various countries through their National Space Agencies [1]. Over the past decade, private companies are joining in the efforts to send humans beyond Low Earth Orbit, particularly the Moon and Mars. A clear example is SpaceX who has set very ambitious goals in sending a manned spaced mission to Mars in 2024 [2]. In addition, space tourism, especially sub-orbital, has gained traction. Projects with the aim of consumer space travel have already been initiated by the likes of Virgin Galactic and Blue Origin to name a few [3].

Nonetheless, there are various risks associated with space activity. One of these risks or hazards is related

to the occurrence of fires. Spacecraft are not exempt from suffering a fire, as demonstrated by several fire-related incidents on the Mir station and on the Space Shuttle Programme [4,5]. The most critical incident occurred on Mir station in 1997 [6]. From the fire that occurred in the Apollo mock-up in 1966, which had a fatal outcome for three astronauts, the lesson learned was that it is practically impossible to avoid all types of ignition sources on Spacecraft [7]. With an effervescent space activity taking place in the years to come, the duration of the mission will be extended increasing the probability of fire occurrence. The risk of fire will also increase with the continued use of new materials and off the shelf appliances and technologies.

The current fire safety strategy for spacecraft relies heavily on the passive approach or material selection. Materials for spacecraft applications are selected based on their thermal response to flame spread. To assess the flammability of materials the NASA standard test STD-6001 Test 1 [8] is employed over flat materials. In Test 1, a vertical flat sample of 20 x 5 cm in dimensions is exposed to an ignition source in the bottom part. If the upwards vertical propagation of flame spans more than 15 cm in burnt length, the sample material fails the test and is deemed flammable and unsafe to be used in spacecraft design.

Such a pass/fail criterion test method has been criticised owing to its lack of fundamental understanding of the fire behaviour [9]. In addition, the test is conducted under Earth-gravity conditions, where the flame spread is predominately driven by buoyancy. On the contrary, on spacecraft, there are other variables that could potentially affect the fire behaviour of solid materials such as the forced flow, oxygen concentration and ambient pressure [10].

Despite decades of solid combustion research in microgravity, there are still many unknowns in the fire behaviour of solid materials in microgravity environments. There is an ongoing joint project (NASA, ESA, JAXA, CNES, DLR and others) with the aim of further understanding material flammability in microgravity and to introduce a better standard test method for material selection [10]. The project is called the Spacecraft Fire Experiments (Saffire). Therefore, various researchers across the globe are conducting experimental studies in various microgravity research platforms. From these ongoing studies, the Saffire experiments are conducted on the space cargo Cygnus where the largest samples in dimension in microgravity conditions have been burnt to date [9].
During the Saffire II experiment, various materials were used in the experimental matrix including silicone membrane sheets. However, the four silicone sheets did not achieve ignition and flame spread [11]. This output cannot lead to conclude that silicone-based materials are not flammable in microgravity environments. Such an output was contrary to most of the previous experimental work conducted in microgravity. In previous studies, it was found that the flammability of materials is further increased in microgravity environments from Earth-buoyancy situations [10]. It seems that the silica-ash (SiO_2) formation during the burning of the silicone material is the culprit of the ill-fated output of the Saffire II experiment. It is known that the silica-ash can deposit upstream from the pyrolysis zone, and the accumulated silica-ash can hinder pre-heating and combustions due to its insulating properties [12].

The PDMS is a membrane that acts as a barrier to liquids whereas it is permeable to gaseous elements. These gas permeable/ liquid impermeable membranes are commonly used in laboratory experiments and medical research (catheters, implants, valves, gaskets, etc.). Due to their properties, the PDMS membranes are also of great interest for spacecraft and extra-planetary applications such as life support systems and as wire insulation materials [13]. An experimental study is being carried out with the aim of increasing the fire behaviour understanding of silicone materials. In the experimental study presented herein, silicone membrane rubbery polymer polydimethylsiloxane (PDMS) of various thicknesses were employed. The membranes were ignited, and the flame spread behaviour was observed under opposed and concurrent forced flows. If the flame travels against a flow, it is commonly referred to as the upwards or concurrent case. When the flame travels against a flow, then it is called opposed or downwards. The details of the experimental proceedings are presented in the following.

2. Methodology

The PDMS silicone membrane samples were tested under buoyancy and forced flow conditions. Various parameters were measured during the execution of the experiments; these were the flame spread rates, temperatures and silica-ash deposit. The variables studied only concerned the sample thickness, and the flame spread direction with respect to the buoyant or forced flow, opposed and concurrent.

The silicone membrane samples had a length of 30 cm, a width of 5 cm, and various thicknesses (0.125, 0.25, 0.36 and 0.61 mm). The samples used had an identical formulation as those used in the Saffire II experiment, and they are identified as SSP-M823 from the provider. The burning rate of this silicone is relatively low with

typical heat release rates in the range 60 – 150 kW/m^2, and the materials' operating temperature range is -70˚C – 200˚C. The material properties for the silicone membrane are listed in Table 1.

Table 1 – Various physical properties of the silicone membrane [14].

Property	Value	Property	Value
$\boldsymbol{\rho_s}$	970 kg/m^3	T_v	673 K
$\boldsymbol{\lambda_s}$	0.2 W/mK	c_s	1050 J/kgK

The experiments were conducted in a flow tunnel rig that was designed and constructed for this experimental project, see Figure 1. The main goal of the rig's design was to control a laminar flow in the area where the sample was located since the forced flow was one of the main variables in the current study. The dimensions of the flow chamber were also designed to avoid friction from walls in the area near the sample holder. A fan located in the bottom part of the rig generated the forced flow. Above the fan, an aluminium honeycomb was placed to straighten the flow.

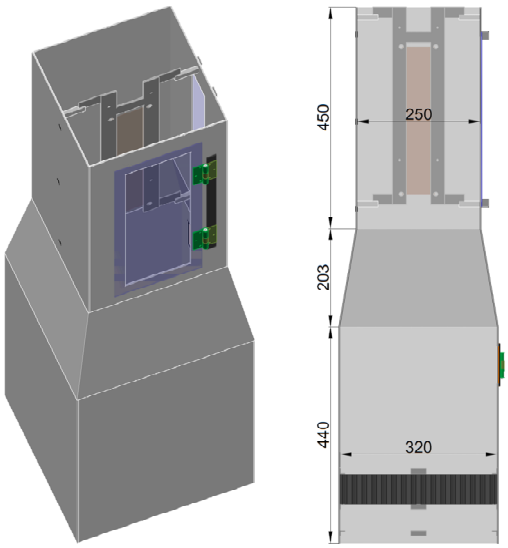

Figure 1 – 3D view (left pane) and longitudinal section (right pane) of the Flow tunnel apparatus.

During the design process, computational fluid dynamics simulations were performed in Autodesk Simulation Software to ascertain a laminar flow in the chamber. In the final design of the rig, the simulations yielded laminar flows in the region close to the sample rig, as expected. In addition, once the flow tunnel rig was completed, a hot wire anemometer measured the flow and confirmed that the forced flow was laminar up to 75 cm/s. Thereafter, the flow started to behave as turbulent.

The flow was controlled using a potentiometer connected to the fan. In turn, a voltmeter was connected to the potentiometer and it could give the voltage readings as the forced flow was regulated by the potentiometer. Hence, the flow was calibrated as a function of the voltage readings and the velocity reading provided by the anemometer. The components of the forced flow system can be seen in Table 2.

Table 2 – Forced flow system components.

Component	Model
Power supply	RS Pro MDR-60 Series
Fan Controller	San Ace PWM
Fan blades	Ebm-papst A series, Ø 200mm
Fan motor	Ebm-papst M4S 068-BF
Anemometer	KIMO CTV 210

To achieve ignition during the experiments, a 29 AWG Kanthal wire was used. The wire was coiled with a diameter of 6 cm. The coiled wire was connected to the AC/DC power distributor; hence, the minimum amount of energy was delivered to achieve ignition. The temperatures were measured with nine Ø 1.2 mm type K thermocouples. The thermocouples were discretely positioned to allow the measurement of the gas-phase and solid-phase at different locations across the sample.

A video camera was used to record the flame spread during the experiments in the flow chamber. Two openings were located in the frontal and lateral side to allow for visual measurements. One of these openings was openable and was needed to place the sample holder inside the chamber. The video recordings were subsequently analysed with a MatLab script that converts certain frames from the video into a binary code. Based on the discrimination of white pixels (flames) from the rest of black pixels in each frame, the flame edges can be tracked as a function of time. Then, the flame spread rate can be easily estimated based on the flame edge position when steady.

During the upwards (concurrent) flame spread experiments, it was expected that the silica ash would deposit on the material surface as the burning progressed. This silica-ash deposit was expected to influence the combustion process significantly enough to cause extinction. Therefore, in the experiments where flame did not spread along the entire length of the sample, the silica-ash deposit was measured from the point of extinguishment. The distance from the point of extinguishment upwards is defined as X_{ext}.The quantification of the silica-ash deposit was done by taking various small samples, from the post-burn silicone membrane sheet, to be measured in a Scanning Electron Microscope (SEM).

3. Theoretical background

The fire behaviour of solid materials is analysed through the flame spread over the silicone samples in the various experimental conditions. Flame spread is considered to be a concatenation of various ignitions. During ignition, when the material is heated up, either by an external source or the flame, the unburnt material starts to decompose and gases emanate (pyrolysis). These gases accumulate over the sample surface and mix with the oxidizer resulting in a flammable mixture. The flammable mixture reaches a certain temperature (vaporisation) that allows for an exothermic reaction to occur under the stimulus of an external source (spark or flame). Depending on the configuration of the flame spread, concurrent of opposed, the leading mechanisms vary and are also influenced by environmental factors.

Flame spread under opposed or downwards laminar flow is dominated by the leading edge (heat conduction from the gas-phase to the solid-phase), see Figure 2. In the concurrent or upwards case, the flame spread is dominated by the length geometry and the characteristics of the flame such as flame length, flame thickness, and soot level, as shown in Figure 3.

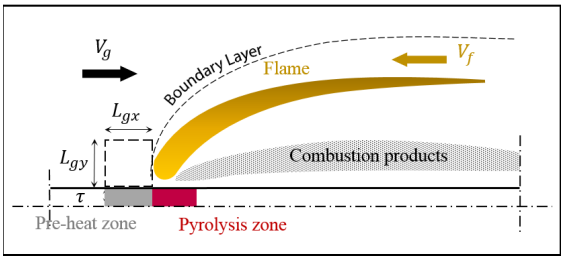

Figure 2 – Schematic diagram of a flame spread in opposed flow and the characteristic lengths.

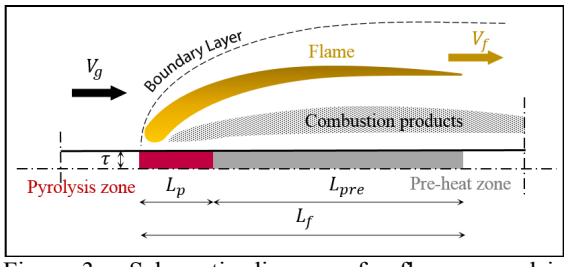

Figure 3 – Schematic diagram of a flame spread in concurrent flows and the characteristic lengths.

The formulae that can be used to describe and predict the flame spread rate for each case are explained in detail in the following sections. But firstly, the thermal behaviour of each sample is defined in the following.

2.1. Defining the thermal behaviour

The thermal behaviour of a material during combustion can be defined according to the thermal gradient within the material. A solid material can behave as thermally thin when the temperature in the solid-phase is uniform; this is typical of very thin materials. On the contrary, for thicker materials, there is a thermal gradient with the solid-phase. These materials are classified as thermally thick. Such a thermal behaviour has a significant impact on the burning and flame spread behaviour of solid materials. Therefore, it is important the determination of the thermal behaviour of the PDMS membrane samples for this experimental study. One method to determine the thermal behaviour is by estimating the Biot number, see Equation 1. The Biot number is a dimensionless ratio of the heat transfer resistance inside and at the surface of the body. A Biot number much lower than unity ($Bi \ll 1$) indicates that there is no thermal gradient within the solid (thermally thin behaviour), whereas if Bi is not much lower than unity t,hen the thermal gradient within the solid should be consider [15].

$$Bi = (h_c l_r)/\lambda_g \qquad \text{Equation 1}$$

Taking into account the sample thickness, and using Equation 1, it yields Bi numbers of 0.02, 0.04, 0.06 and 0.11 for the samples thicknesses of 0.125, 0.25, 0.36 and 0.61 mm, respectively. As such, the samples with the first three thicknesses can be assumed to behave as thermally thin. The sample with 0.61 mm thickness yielded the largest Bi number. Hence it can be assumed that it will behave as thermally thick or it will be transitioning towards thermally thick behaviour.

Nonetheless, the drawback of the Biot number is that it omits other environmental variables, such as the forced flow. Based on dimensional analysis, Bhattacharjee and co-workers [16] established the boundary criterion to determine the thermal behaviour of a sample under opposed forced flows:

$$\tau_{cr} = \frac{\pi}{4}\frac{\lambda_g}{\rho_g c_g V_g \left(\frac{T_f - T_v}{T_v - T_\infty}\right)} \qquad \text{Equation 2}$$

The density and specific heat capacity are evaluated at the temperature of vaporisation of the silicone material, and the temperature is the maximum obtained from the thermocouple readings. Plotting Equation 2 results in a curve as a function of the sample thickness and the opposed forced flow, see Figure 4, and defines the boundary for the thermal behaviour of the silicone samples. As seen in Figure 4, the 0.125 mm and 0.25 mm samples present a thermally thin behaviour since

most of them are located under the curve for the studied forced flows. The 0.36 mm sample behaves as thermally thin but at 46 cm/s forced flow the sample transits from thermally thin to thermally thick. The 0.61mm sample transits from thermally thin behaviour at 26 cm/s forced flow.

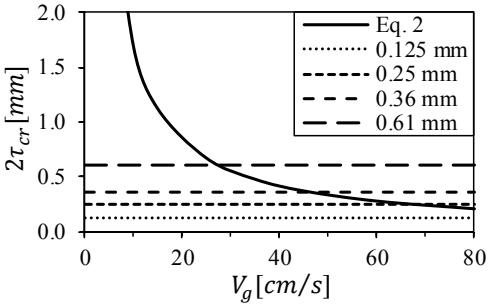

Figure 4 – Estimated critical transition thickness as a function of the opposed forced flow.

For the case of concurrent forced flow, it does not seem to be a boundary criterion established in the literature, to the knowledge of the authors. But equating the flame spread formulae for thermally thin and thick ($V_{f,thin} = V_{f,thick}$) provided by Fernandez-Pello [17], it results in the following thermal boundary criterion under concurrent forced flows:

$$\tau_{cr} = \frac{\pi\lambda_s(T_v - T_\infty)}{4(\dot{q}''_{cf} + \dot{q}''_{fr} - \dot{q}''_{sr})} \qquad \text{Equation 3}$$

Where the convective heat transfer from the flame to the solid surface is:

$$\dot{q}''_{cf} = \left(\frac{\lambda_g \rho_g c_g V_g}{l_p}\right)^{1/2} (T_f - T_v) \qquad \text{Equation 4}$$

As seen, estimating the critical boundary thickness to establish the thermal behaviour of the silicone samples under concurrent forced flows is not trivial. Some input parameters to solve Equation 3 are only obtainable empirically. As such, the thermal behaviour will be based on the Biot number under concurrent forced flows.

2.2. Downwards or opposed flame spread

In the opposed case and for thermally thin fuels, an extended simplified analysis has been proposed [18–20]. With the appropriate simplification and assumptions, a heat balance at the flame front, see Figure 3, can then be established. The energy needed for the fuel to pyrolysate balances the energy from the gas-phase (flame) to solid-phase (pre-heating zone). Then, the following expression to predict opposed flame spread was derived:

$$V_f \sim \frac{\pi}{4}\frac{\lambda_g}{\rho_s c_s \tau}\left(\frac{T_f - T_v}{T_v - T_\infty}\right) \qquad \text{Equation 5}$$

Equation 5 shows resemblance to the De Ris expression [21]. This expression is only valid for a steady flame spread away from extinction. Notice that conduction from the gas-phase to the solid-phase at the leading edge of the flame is the only driving mechanism.

Only two samples, 0.125 mm and 0.36 mm, were studied under concurrent forced flows. The former sample is considered to behave as thermally thin. In the case of the 0.36 mm sample, this will be considered thermally thin since the transition into thermally thick behaviour is expected not to take place up until very large forced flows.

2.3. Upwards or concurrent flame spread

As discussed, flame spread under concurrent forced or buoyant flow is dominated by the flame geometry and affects the flame spread process differently when compared to the opposed flow case. During concurrent flame spread, the total length of the flame affects the solid fuel as this gets heated and vaporises in much larger proportion than under opposed forced flow. Hence, concurrent or upwards flame is faster than the opposed flame spread. Fernandez-Pello [17] established an equation for flame spread under concurrent forced flow for thermally thin materials:

$$V_f = \frac{\left[\dot{q}''_{cf} + \dot{q}''_{fr} - \dot{q}''_{sr}\right](l_{pre})}{\rho_s c_s \tau (T_v - T_\infty)} \qquad \text{Equation 6}$$

And for thermally thick materials:

$$V_f = \frac{4\left[\dot{q}''_{cf} + \dot{q}''_{fr} - \dot{q}''_{sr}\right]^2(l_{pre})}{\pi\rho_s c_s \lambda_s (T_v - T_\infty)} \qquad \text{Equation 7}$$

As seen, Equation 6 and Equation 7 present challenges and are quite complex compared to Equation 5. Convection and radiation from the flame to the solid, and surface re-radiation are incorporated into the heat balance. In addition, two characteristic lengths (flame and pre-heat zone) are important input parameters in Equation 6 and Equation 7. For the silicone sample, some of the input parameters to estimate the flame spread are not known and are difficult to determine. Due to the silica-ash formation and deposit upstream from the pyrolysis zone during the combustion, the convective and radiative heat flux from the flame received at the solid surface will be affected. Also, the silica-ash will affect the surface re-radiation and other mechanisms behind flame spread.

4. Results and Discussion

In the following section, the results are presented and discussed. In the first section, the flame temperature measurements are introduced. In the second section, the burnt length during concurrent and opposed buoyant and forced flows are presented. In the third section, the flame spread results and predictions are discussed. Finally, in the last section, the results concerning silica-ash formation are introduced and discussed with estimations of the heat flux balance.

4.1. *Flame temperature*

Initially, the thermocouples were discretely placed so as to measure gas-phase (flame) and solid-phase (pyrolysis zone) temperatures. However, the temperature readings quickly showed that it was impossible to measure the solid-phase temperatures as the material deformed during pre-heating. As a consequence, the selected locations on the material surfaces were misplaced with respect to the thermocouples. Figure 5 depicts only the thermocouple measurements for the gas-phase, and thermocouple T8 measured the maximum flame temperature which was 1149 ˚C (1422 K). This maximum temperature is equivalent to a linearized temperature for the measurements, and it will be later used to estimate the flame spread.

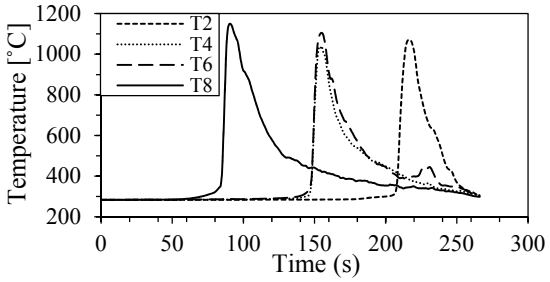

Figure 5 – Measured flame temperatures readings for a downwards buoyant experiment.

4.2. *Burnt length*

The burnt length results from various scenarios and from a previous study [14] are depicted in Figure 6. For sample thicknesses of 50 mm, the burnt length differed greatly for the concurrent flame spread at buoyant conditions (no forced flow). As the thickness of the sample increases, the burnt length decreases, see left pane in Figure 6. Similar qualitative results were found by Niehaus et al. [14]. The results obtained in this study passed the criterion from Test 1, whereas two samples from Niehaus et al. [14] did not pass the criterion. This quantitative difference shows that test 1 results are influenced by the execution method and the operator. The burnt lengths results under downwards flame spread are shown in the right pane in Figure 6. As seen, the burnt length in two sample thickness (0.25 mm and 0.36 mm) exceeded 15 cm and did not pass Test 1, whereas only the 0.61 mm sample passed the criterion.

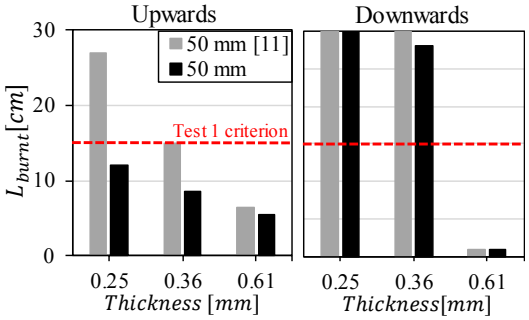

Figure 6 – Burnt length results from upwards and downwards flame spread at no forced flow for the silicone samples (buoyant conditions).

Under concurrent forced flows, the burnt length is also affected by the flow velocity as shown in Figure 7. The experiments conducted under forced flow conditions resulted in a distinctive behaviour as a function of the sample thickness. The sample with 0.61 mm resulted in a burnt length decreasing linearly with increasing forced flow velocity. On the contrary, the burnt lengths from the 0.25 mm and 0.36 mm samples exhibited a non-monotonic behaviour with maximum burnt lengths obtained at 35 cm/s forced flow as seen in Figure 7. It seems that the silica-ash formation upstream from the pyrolysis zone under forced flow might have an effect in this distinctive behaviour.

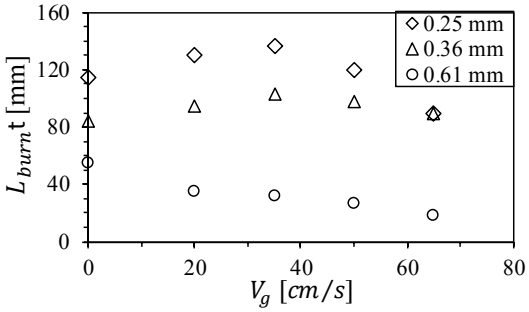

Figure 7 – Burnt length as a function of the forced flow for various thickness of 5 cm wide samples.

4.3. *Flame spread rate*

Natural buoyancy generates a characteristic relative flow when a flame develops and spreads that will depend on the thermal characteristic of each solid material. An expression from Bhattacharjee et al. [16] can be used to estimate the characteristic buoyancy-driven flow.

$$V_{nb} = \left[\left(\alpha_g g\left(T_g - T_\infty\right)\right)/T_\infty\right]^{1/3} \qquad \text{Equation 8}$$

In Equation 8, the gas-phase temperature and gas-phase thermal diffusivity are evaluated at T_v of the silicone sample. Then, for the silicone sample, the buoyancy driven flow is 10.5 cm/s. The forced flow velocities in the flame spread results were then corrected by adding the buoyancy relative flow, see Figure 8.

Figure 8 depicts the flame spread results as a function of the corrected forced flow under opposed and concurrent scenarios. In the opposed case, the flame spread rate results for two sample thicknesses were independent of the forced flow, as it is expected to occur for the range of forced flow studied [22]. Based on the silicone properties, predictions were made with Equation 5, which is also shown in Figure 8. The prediction made by Equation 5 compared satisfactorily with the experimental results.

For the concurrent case, the flame spread results show quite a different behaviour with respect to the opposed flow case, see Figure 8. The sample with 0.61 mm thickness resulted in flame spread rates decreasing linearly as a function of the concurrent forced flow. The other sample thicknesses, 0.125 and 0.36 mm, showed a non-monotonic flame spread behaviour as a function of the forced flow. The maximum flame spread was attained at 30 cm/s. This behaviour was previously observed with the burnt length results. Again, the silica-ash formation seems to affect the pre-heat region upstream from the pyrolysis area. No predictions were made for the concurrent flame spread, as some input parameters remain unknown. Also, as the silica-ash deposits on the solid surface, this layer of silica-ash has to be taken into account in Equation 6, which complicates any prediction even further.

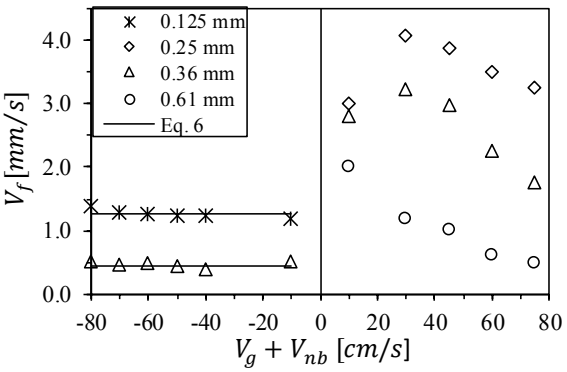

Figure 8 – Flame spread rate results as a function of opposed (negative axis) and concurrent (positive axis) corrected forced flow.

4.4. Silica-ash deposition

As seen in the previous results under concurrent forced flows, the silica-ash formation upstream from the pyrolysis zone plays a substantial role in the flame spread behaviour. Therefore, a SEM was used to quantify the silica-ash thickness upstream from the point of extinguishment (X_{ext}). Figure 9 depicts the silica-ash thickness results for upstream flame spread (buoyant). As seen, the silica-ash thickness is thicker at the point of extinguishment (X_{ext}). Thereafter, the silica-ash thickness decreases exponentially as the distance from the point of extinguishment increases.

The same behaviour was observed for all sample thicknesses under concurrent forced flow. The 0.61 mm sample yielded the thicker silica-ash thickness, and the thinner sample gradually resulted in thinner silica-ash thicknesses. Such behaviour seems to be logical as a thicker sample would result in an increasing amount of silica-ash during combustion. Due to this increased production of silica-ash, the burnt lengths for the 0.36 mm thickness were low.

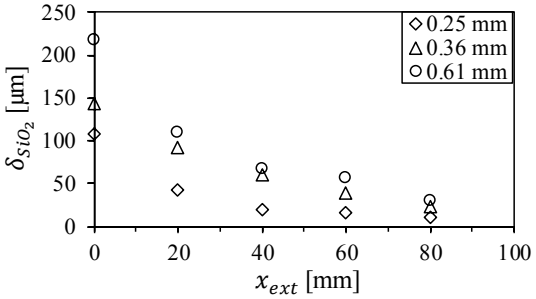

Figure 9 – Silica-ash thickness downstream from the point of extinguishment in buoyant conditions for various sample thicknesses.

The silica-ash formation as a function of the forced flow at various distances from the point of extinguishment is depicted in Figure 10. As seen, in the 0.36 mm sample, the silica-ash thickness decreased with increasing forced flow in a linear manner at $X_{ext} = 0$ mm (point of extinguishment) and at $X_{ext} = 60$ mm. However, at other distances from the point of extinguishment, the silica-ash thickness showed a non-steady behaviour as the forced flow increased ($X_{ext} = 20, 60$ and 80 mm). Likewise, similar non-monotonic behaviour in the silica-ash thickness was observed in the 0.61 mm sample. Such a heterogeneous behaviour in silica-ash formation with respect to the forced flow might be owing to the warping and deformation behaviour of the silicone samples during combustion. From Figure 10 it is also clear that the largest accumulation of silica-ash occurs within the first 20 mm from the point of extinguishment.

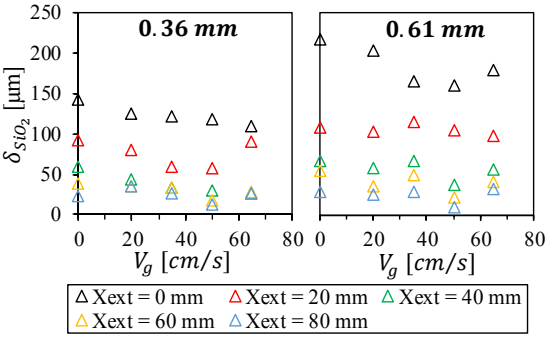

Figure 10 – Silica-ash deposit thickness downstream from the point of extinguishment as a function of forced flow for a 0.36 mm sample (left pane) and a 0.61 mm sample (right pane).

Average silica-ash thickness as a function of the forced flows was calculated to account for the total silica-ash formation downstream from the point of extinguishment, and the results are shown in Figure 11. The 0.36 mm and 0.61 mm samples resulted in decreasing average silica-ash thickness up to a 50 cm/s forced flow. Thereafter, the silica-ash thickness increased in thickness for both silicone samples. In the case of the 0.25 mm sample, the average silicone increased slightly with increasing forced flow up to 35 cm/s and decreased after that. In addition, in terms of the average silica-ash thickness, the silica-ash formation increased with increasing sample thickness. These average results indicate that the forced flow affects the silica-ash formation non-monotonically.

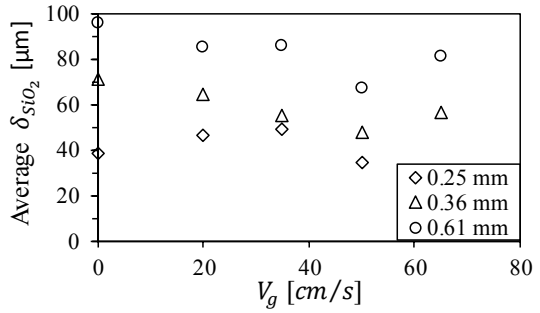

Figure 11 – Average silica-ash deposit as a function of the forced flow for various samples with various thicknesses.

A ratio of the silica-ash thickness to the half thickness of the sample was calculated to better account the effect of the forced flow on the silica-ash formation. This ratio is depicted in Figure 12 as a function of the forced flow at $X_{ext} = 0\ mm$ and $X_{ext} = 20\ mm$. At the point of extinguishment, see left pane in Figure 12, the ratio decreased almost linearly with increasing forced flow for the three samples. In general, it was observed that the ratio decreased slightly with increasing sample thickness. Nonetheless, the dependency of the ratio with respect to the forced flow at 20 mm from the point of extinguishment seemed not to hold, see the right pane in Figure 12. In the 0.25 mm and 0.36 mm samples, the ratio increased or decreased with increasing forced flow. Whereas, the ratio remained almost independent from the forced flow in the 0.61 mm sample. As seen, the forced flows seems to have a strong effect on the silica-formation at the point of extinguishment. But away from this point, the silica-ash formation seems to be affected by other aspects of the material behaviour. During the execution of the experiments, it was observed that the silicone sample warped and deformed as it was heated up by the flames.

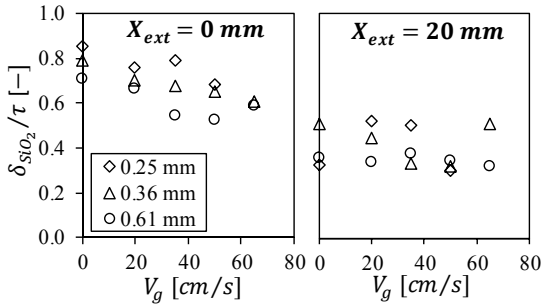

Figure 12 – Ratio of silica-ash thickness to the half thickness of the sample as a function of the forced flow at two distances from the point of extinguishment.

Based on the previous results, the silica-ash formation at the point of extinguishment can also indicate part of the extinction mechanisms. At this point, the silica-ash accumulation might have hindered the underlying layer of silicone to heat up and thus lead to the extinction of the upwards flame spread. Accounting only the thermal consequences of the silica-ash formation during the burning process, the critical heat flux needed to vaporise the virgin silicone fuel and the silica-ash layer at the point of extinguishment was estimated. The following expression was used to estimate the critical heat flux:

$$\dot{q}''_{crit} = \frac{\left[(\rho_s c_s \tau) + \left(\rho_{SiO_2} c_{SiO_2} \delta_{SiO_2}\right)\right](T_v - T_\infty)}{Burning\ time}$$

Equation 9

The burning time was taken as average for the various repetitions for each sample thickness. The critical heat flux was calculated based on the silica-ash thickness measurements at the point of extinguishment and on the average burning times. Figure 13 depicts the critical heat flux as a function of the concurrent forced flow for various thicknesses of silicone. For each sample thickness, the critical heat flux is highest at no forced flow (natural buoyancy). These results were

expected as the silica-ash thickness was greatest at buoyant flow conditions. The critical heat flux decreases as the forced flow increases to 20 cm/s. Nevertheless, with further increasing of forced flow, the critical heat flux seemed to remain quasi-constant or decreased slightly. It seems that the silica-ash formation has a greater impact at buoyant conditions. As the forced flow aids the upwards flame spread, silica-ash is dispersed with reduced thickness. The estimated critical heat flux is reduced, and in turn, larger burnt lengths are produced as seen in Section 4.2. Solving the problem cannot just be reliant on the thermal approach. Kinetics may also explain the extinction mechanisms that require further investigation since in this study the problem was only treated from a thermal point of view.

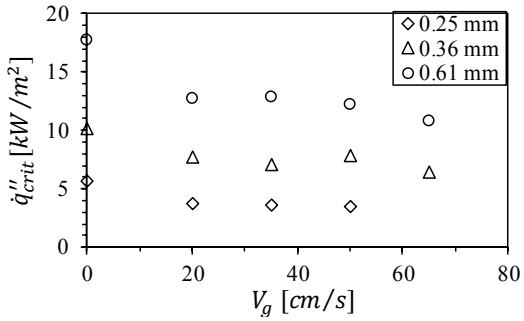

Figure 13 – Critical heat flux at the point of extinguishment as a function of the forced flow.

6. Conclusions and further work

An experimental study was conducted to study the flame behaviour of PDMS membrane sheets of various thickness under concurrent and opposed buoyant and forced flows. In addition, the silica-ash formation was quantified by measuring the thickness of post-burnt samples in a SEM.

The burnt length results showed the drawbacks of using the criterion from the NASA Test 1 standard. Under concurrent forced flows, the burnt length showed a linear (0.61 mm sample) and non-monotonically (0.25 and 0.36 mm) dependency on the forced flow.

The flame spread rate under opposed forced flow exhibited an independent behaviour from the range of forced flows studied and for two thermally thin samples. This behaviour complies with theory. Prediction using an equation based on scaling approach resulted in good accuracy with respect to the opposed flame spread. For the concurrent forced flows, the flame spread rates showed a non-monotonically dependency for the 0.25 mm and 0.36 mm samples. For the 0.61 mm samples, the flame spread rates exhibited a linear decreasing behaviour with increasing forced flow. No predictions were possible for the concurrent flame spread since the silica-ash formation made difficult to compute some of the input parameters in the corresponding formulae.

Quantification of the silica-ash formation downstream from the point of extinguishment showed various distinctive behaviours as a function of the forced flow. The measurements indicated that the silica-ash accumulated mostly along the first 20 mm upwards from the point of extinguishment. In absolute terms, the silica-ash thickness showed non-monotonically dependency on the forced flow. When looking into at the ratio of silica-ash thickness to the half thickness of silicone, the results showed an almost linear dependency on the forced flow at the point of extinguishment. However, at 20 mm downwards from the point of extinguishment, the dependency was not clear. It seems that the deformation of the silicone samples during burning also influenced the silica-ash formation.

The critical heat flux needed to raise the temperature of the silicone layer to sustain flame spread was estimated at the point of extinguishment. The estimated critical heat flux was greatest under buoyant conditions (no forced flows), decreased with a 20 cm/s increase in forced flow. With further increasing forced flows, the critical heat flux exhibited almost none dependency. These results indicate that the concurrent flame spread on silicone samples are not only a thermal issue, kinetics should also be accounted for in future studies.

In the future, further experiments will take place to elucidate the mechanisms behind flame spread and extinction of PDMS materials during opposed and concurrent forced flows. The next study will also focus on the fundamental aspects of combustion of solid materials, and it will provide a more robust flammability assessment of PDMS materials for spacecraft applications.

Acknowledgements

The authors would like to express their gratitude to the support from the topical team on fire safety in space (ESTEC contract number 4000103397). Special gratitude is shown to the School of Engineering at the University of Edinburgh for the financial support for Ulises Rojas Alva's PhD.

References

[1] J. Thomas, Privatization of Space Ventures: Proposing a Proven Regulatory Theory for Future Extraterrestrial Appropriation Recommended

Citation, 2005. https://digitalcommons.law.byu.edu/cgi/viewcontent.cgi?article=1006&context=ilmr (accessed October 5, 2018).

[2] Making Life Multiplanetary | SpaceX, (n.d.). https://www.spacex.com/mars (accessed October 5, 2018).

[3] Branson Aims Mid-2018 Space Trip as Virgin Resumes Powered Tests - Bloomberg, (n.d.). https://www.bloomberg.com/news/articles/2017-07-05/branson-targets-space-by-mid-2018-as-virgin-begins-powered-tests (accessed October 5, 2018).

[4] F.L. Thompson, F. Borman, M.A. Faget, E.B. Geer, C.F. Strang, R.W.V. Dolah, G.C. White, J.J. Williams, Report of Apollo 204 Review Board, Washington, D.C., 1967.

[5] R. Friedman, S.A. Gokoglu, L. Urban, David, Microgravity combustion research: 1999 Program and Results, Cleveland, Ohio, 1999.

[6] S.D. Egorov, B.A. Yu, L.P. Klimin, V.S. Voiteshonok, A. V Ivanov, A. V Semenov, E.N. Zaitsev, E. V Balashov, T. V Andreeva, Fire safety experiments on "MIR" orbital station, in: Third Int. Microgravity Combust. Work., National Aeronautics and Space Administration NASA, Cleveland, Ohio, 1995: pp. 195–200.

[7] J.F. Lewis, R. Barido, G.C. Tuan, Crew Exploration Vehicle Environmental Control and Life Support Fire Protection Approach, in: 37th Int. Conf. Environ. Syst., Chicago, Illinois, 2007. doi:10.4271/2007-01-3255.

[8] NASA, Flammability, offgassing, and compatibility requirements and test procedures. NASA-STD-6001B, (2016) 1–158.

[9] G. Jomaas, J.L. Torero, C. Eigenbrod, S.L. Olson, P. V. Ferkul, G. Legros, A.C. Fernandez-Pello, A.J. Cowlard, S. Rouvreau, N. Smirnov, O. Fujita, J.S. T'ien, G.A. Ruff, D.L. Urban, Fire Safety in Space – Beyond Flammability Testing of Small Samples, Acta Astronaut. 109 (2015) 208–216.

[10] O. Fujita, Solid combustion research in microgravity as a basis of fire safety in space, Proc. Combust. Inst. 35 (2015) 2487–2502.

[11] P. Ferkul, S. Olson, D.L. Urban, G.A. Ruff, J. Easton, J.S. T'ien, Y.-T.T. Liao, A.C. Fernandez-Pello, J.L. Torero, C. Eigenbrod, G. Legros, N. Smirnov, F. Osamu, S. Rouvreau, B. Toth, G. Jomaas, Results of Large-Scale Spacecraft Flammability Tests, in: 47th Int. Conf. Environ. Syst. ICES, 2017.

[12] F.-Y. Hshieh, Shielding effects of silica-ash layer on the combustion of silicones and their possible applications on the fire retardancy of organic polymers, Fire Mater. 22 (1998) 69–76.

[13] P. Jha, J.D. Way, A. Srinivasan, L.W. Mason, Membranes on Mars for In-Situ Resource Utilization Processes, in: 2004. doi:10.4271/2004-01-2316.

[14] J.E. Niehaus, P. V Ferkul, S.A. Gokoglu, G.A. Ruff, Buoyant Effects on the Flammability of Silicone Samples Planned for the Spacecraft Fire Experiment (Saffire), in: 45th Int. Conf. Environ. Syst. 12-16, Bellevue, Washington, 2015.

[15] M.J. Hurley, D. Gottuk, J.R. Hall, K. Harada, E. Kuligowski, M. Puchovsky, J. Torero, J.M. Watts, C. Wieczorek, eds., SFPE Handbook of Fire Protection Engineering, 5th editio, Springer, 2016. doi:10.1007/978-1-4939-2565-0.

[16] S. Bhattacharjee, M. Laue, L. Carmignani, P. Ferkul, S. Olson, Opposed- flow flame spread: A comparison of microgravity and normal gravity experiments to establish the thermal regime, Fire Saf. J. 79 (2016) 111–118. doi:10.1016/j.firesaf.2015.11.011.

[17] C.A. Fernandez-Pello, The Solid Phase, in: G. Cox (Ed.), Combust. Fundam. Fire, Academic Press, 1995: pp. 29–100.

[18] S. Takahashi, M. Kondou, K. Wakai, S. Bhattacharjee, Effect of radiation loss on flame spread over a thin PMMA sheet in microgravity, Proc. Combust. Inst. 29 (2002) 2579–2586. doi:10.1016/S1540-7489(02)80314-5.

[19] S. Bhattacharjee, K. Wakai, S. Takahashi, Flame spread in a microgravity environment - Role of fuel thickness, in: Sixth Int. Microgravity Combust. Work., National Aeronautics and Space Administration NASA, Cleveland, Ohio, 2001: pp. 405–408.

[20] S. Bhattacharjee, C. Paolini, K. Wakai, S. Takahashi, Extinction criteria for opposed-flow flame spread in a microgravity environment, in: Seventh Int. Work. Microgravity Combust. Chem. React. Syst., National Aeronautics and Space Administration NASA, Cleveland, Ohio, 2003: pp. 201–204.

[21] J.N. De Ris, Spread of laminar diffusion flame, Symp. Combust. 12 (1969) 241–252.

[22] A.C. Fernandez-Pello, S.R. Ray, I. Glassman, Flame spread in an opposed forced flow: the effect of ambient oxygen concentration, Eighteenth Symp. Combust. 18 (1981) 579–589. doi:10.1016/S0082-0784(81)80063-X.